Title
Ultrafast study of phonon transport in isotopically controlled semiconductor nanostructures

Journal
physica status solidi (a) – applications and materials science, 213(3)

ISSN
1862-6300

Authors
Issenmann, Daniel
Eon, Soizic
Bracht, Hartmut
et al.

Publication Date
2016-03-01

DOI
10.1002/pssa.201532462

Peer reviewed

Wiley Online Library
Early View publication on www.wileyonlinelibrary.com
(issue and page numbers not yet assigned;
citable using Digital Object Identifier – **DOI**)

Phys. Status Solidi A, 1–8 (2015) / **DOI** 10.1002/pssa.201532462

Part of Special Issue on
German Priority Program DFG-SPP 1386
Nanostructured Thermoelectrics (2009-2015)

physica status solidi a
www.pss-a.com
applications and materials science

Ultrafast study of phonon transport in isotopically controlled semiconductor nanostructures

Daniel Issenmann[1], Soizic Eon[2], Hartmut Bracht[2], Mike Hettich[3], Thomas Dekorsy[3], Gernot Buth[1], Ralph Steininger[1], Tilo Baumbach[1,4], John Lundsgaard Hansen[5], Arne Nylandsted Larsen[5], Joel W. Ager III[6], Eugene E. Haller[6], and Anton Plech[*,1]

[1] Institute for Photon Science and Synchrotron Radiation/ANKA, Karlsruhe Institute of Technology, PO box 3640, 76021 Karlsruhe
[2] Institute of Materials Physics, University of Muenster, Wilhelm-Klemm-Strasse 10, 48149 Münster
[3] Center for Applied Photonics and Department of Physics, University Konstanz, Universitätsstr. 10, 78262 Konstanz
[4] Laboratory for Application of Synchrotron Radiation, Karlsruhe Institute of Technology, PO Box 3640, 76021 Karlsruhe
[5] Department of Physics and Astronomy, Ny Munkegade 120, University of Aarhus, 8000 Aarhus, Denmark
[6] Lawrence Berkeley National Laboratory, 1 Cyclotron Road, Berkeley, CA 94720, USA

Received 30 June 2015, revised 9 October 2015, accepted 14 October 2015
Published online 5 November 2015

Keywords femtosecond spectroscopy, Ge, multilayers, Si, thermal conductivity, ultrafast X-ray scattering, zone folding

[*] Corresponding author: e-mail anton.plech@kit.edu, Phone: +49-721-60828665, Fax: +49-721-60828677

Isotopically modulated silicon and germanium multilayers are analyzed by means of femtosecond spectroscopy and pulsed X-ray scattering for determining thermal conductivity and phonon modes. Isotopic modulation decreases thermal conductivity stronger than expected from a band bending model in the coherent phonon transport regime, in particular for silicon. Femtosecond spectroscopy and X-ray scattering resolve zone-folded vibration modes, which are located at the edge of the new, smaller Brillouin zone due to the multilayer periodicity. These modes can contribute to the reduction of thermal conductivity by *Umklapp* processes within the zone-folded mini-bands.

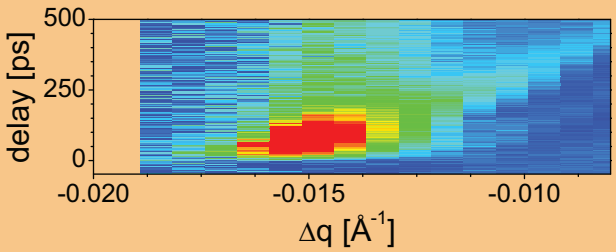

Color-coded increase in ultrafast X-ray scattering in vicinity to the mini-zone boundary of a germanium multilayer.

1 Introduction Highly crystalline, pure semiconductor materials are not very suitable as thermoelectric materials due to the high thermal conductivity in bulk. For instance, silicon or germanium, would be highly interesting in integrated applications in thin-film technology, where contamination by foreign elements is undesirable. Yet, the thermal conductivities of 145 for silicon, respectively, 60 W/(m·K) for germanium at room temperature are up to two orders of magnitude higher than for common thermoelectric materials with high efficiency. This only improves at higher temperatures [1]. The thermal conductivity κ, in turn, is one of the contributions to the thermoelectric figure-of-merit $ZT = S^2\sigma T/(\kappa_e + \kappa_l)$ with S, σ, T, and $\kappa_{e,l}$ being Seebeck coefficient, electrical conductivity, temperature and thermal conductivity (electronic and lattice contribution).

Nevertheless, well-defined crystals allow for a sensitive study of the mechanisms for tuning thermal conductivity. We study single-crystalline silicon and germanium thin films grown by molecular beam epitaxy, where alternating isotopically pure layers modulate the phonon transport. In fact such structures behave electronically as unperturbed bulk materials, while phonons sense the modified mass distribution.

The structural perturbation at the same time is weak (strain is virtually absent) and mechanisms of phonon interactions may be disentangled.

The isotopic modulation may be seen as a scattering center for phonons, changing their momentum and causing thermal resistance. This happens naturally in most materials with different stable isotopes and is an additive incoherent effect. A periodic modulation, however, may induce an interaction that goes beyond incoherent scattering processes and might involve phonon–phonon interactions with coherent contributions. In this case, influence on thermal transport is far from being trivial and might open up ways for tailoring the thermal conductivity.

Despite, the demonstrations of successful coherent transport modulation in, for instance, multilayered thin-film samples are rare [2–4]. An accepted notion involves a change in transport properties of the system while changing the characteristic size of the modulation, i.e., the multilayer period. Naturally, starting with long periods, the effect on thermal conductivity is low, simply due to the low number of interfaces. As period decreases thermal conductivity decreases as well. Instead of reaching a limit (e.g., the alloy limit of complete disorder) eventually conductivity would rise again for the smallest periods. In the most general explanation this comes from the fact that transport is mediated to large extent by long-wavelength phonons. These phonons do not sense the heterogeneity due to their limited localization. Consequently, a minimum in thermal conductivity at finite multilayer period is observed [4–7]. Much less agreement is found in literature on explaining part of these effects in terms of phonon band blockage [8–10] or band bending [11] or, as opposed to that, enhanced transport of phonon Bloch waves in these structures (ballistic transport)[4, 12–14].

Artificial multilayers of materials such as AlAs/GaAs [15–18], SiGe [2, 8, 19], $SrRuO_3/SrTiO_3$ [20] or even common thermoelectric materials [6] have been investigated in the past to understand the phonon modifications in such structures. One central observation is that the newly introduced periodicity causes a folding of the phonon branches with larger wave vector into the center of the zone, such that phonon energy is preserved, but phonon momentum is reduced below the new zone boundary [21]. This has early been seen as well in isotopically modulated structures [22, 23] and is now well understood as standing or commensurate waves within the modulated structure. The frequently observed phonon modes are indeed zone center modes that do not propagate [16, 17, 24]. Whether this prevalence is simply due to the usual detection by optical light or related to higher oscillation strength of these modes is not clear.

Here, we present thermal conductivity measurements and ultrafast spectroscopy and X-ray scattering on isotopically modulated silicon multilayers and germanium multilayers in order to investigate this interrelation. Except for the acoustic impedance in these structures being typically much lower than in heterostructures they can be grown as perfect multilayers without additional point scatterers from growth defects. In particular hetero-epitaxial strain can lead to prominent defect inclusion and thus masking of coherent effects.

2 Materials and methods

2.1 Sample preparation Silicon or germanium crystals with isotopically modulated layers starting from 28-Si and 29-Si or 70-Ge and natural germanium, respectively, were epitaxially grown by means of molecular beam epitaxy (MBE) on (100) oriented wafers of natural isotopic abundance. Both semiconductor structures contained 20 bilayers of nominally (10 + 10) nm for a total thickness of about 400 nm for the entire layer structure. X-ray scattering and secondary ion mass spectroscopy revealed a real layer thickness of about 11.3 nm for the germanium sample and 9.7 nm for the silicon sample. Reference samples with a 400 nm epilayer of 28-Si and natural germanium, respectively, were grown as well.

Only for the time-domain conductance measurements the wafers were coated by thin gold films (30 nm) by ion sputtering. Care was taken to perform cleaning and deposition steps of both isotope multilayer and natural epilayer sample in the same batch for a reliable reference state. The gold layer was deposited on top of a thin (3 nm) chromium adhesion layer to improve the interface conductance between metal film and semiconductor [25].

2.2 Femtosecond spectroscopy - ASOPS Asynchronous optical sampling (ASOPS) has been employed to record weak transient optical changes in reflection from the as-grown isotopic multilayer structures. The method has been introduced elsewhere [18], in brief two femtosecond oscillators (Gigaoptics, Germany) are synchronized, but detuned in repetition rate (at about 1 GHz) by a small difference frequency (10 kHz). Thus, the temporal delay of both pulses at the sample changes in a linear fashion in time and can be recorded by a fast photodiode and a transient recorder (GaGe Applied). A high-contrast determination of changes in light reflection at 800 nm due to optical pumping (805 nm) is possible. Beam powers of 35 and 5 mW for pump and probe beams, respectively, are used at a focus of 2.5 μm (pulse fluence 56 J m^{-2}). The reflection angle of the probe beam defines the momentum transfer $q = 4\pi/\lambda \cdot \sin(2\Theta/2)$ of the scattered waves in the language of a Raman-type process (wavelength λ, scattering angle 2Θ). Either 90° or 180° (retroreflection) in 2Θ were set up. No gold coating was used on the semiconductor structures.

The typical electronic contribution was subtracted from the raw curves by simulating the sigmoidal rise and exponential decay in the 1–2 picosecond range. Additionally, subtracting a median of the curve of defined width allowed to remove the low frequency content, after which a Fourier transform shows the spectral power contained in the curves.

2.3 Pulsed X-ray scattering–synchronous Pump–probe X-ray scattering was performed at the European Synchrotron Radiation Facility (ESRF) by employing an amplified Ti:Sa regenerative amplifier (Coherent) as laser

pump source and the time-delayed, but synchronized X-ray pulses from the storage ring as probe pulses. At the beamline ID09 the setup comprises a monochromator at 15 keV and in particular an ultrasonic chopper to reduce the repetition rate of the X-ray pulses down to the 1 kHz repetition rate of the laser [26]. Scattered X-rays close to the Bragg angle of the Si(400), resp. Ge(400) reflection for the uncoated surfaces and at the gold powder (111) peak for the gold-coated samples are recorded on a charge-coupled device (CCD, FReLoN, ESRF Grenoble) with thin-film scintillator. Analysis was done either by in-plane cuts to the scattering distribution or powder-type integration along 2Θ for the gold diffraction. Intensity at the crystal truncation rods was derived for the analysis of the diffuse scattering close to the Bragg peak. The gold powder peaks were analyzed in terms of transient peak shifts, which are translated into temperature change in the gold film [27, 7].

The delay between laser and X-ray pulses can be changed electronically with steps of 5 ps for the complete delay range up to 1 ms. X-ray pulses were typically 70–100 ps long [28]. The excitation was repeated for some 1000 to 3000 pulses for one CCD image with one delay point. In particular the laser fluence for the heating of the gold film at 400 nm had to be controlled precisely in between 8 and 16 J m^{-2} per pulse to remain within the linear heating response of the film [25]. This linear relationship allows for replacing relative lattice expansion with relative temperature change. For sake of brevity, we compared the relative temperature change of the multilayer to that of the reference sample in Fig. 2 to visualize the changes. Thus the initial fast jump in temperature of the heating curve is not visible. Direct excitation of the germanium sample was done at 800 nm with a fluence of 800 J m^{-2}.

2.4 Pulsed X-ray scattering–ASOXS Pump–probe X-ray scattering in asynchronous mode [29, 30] was performed at the ANKA synchrotron, beamline SUL-X by using a high-repetition femtosecond oscillator (500 MHz, 804 nm, Gigaoptics, Germany) as pump source and nearly the same repetition rate of the synchrotron with the asynchronous detuning (25 kHz) as explained above relative to the X-ray pulses. The beating of the X-ray intensity with mutual delay of both sources was recorded by an X-ray avalanche diode (FMB Oxford) and a histogram recorder (Nanoharp, Picoquant). Each temporal delay spectrum was recorded at fixed difference angle from the (400) reflection of Si and Ge to map the transient change of diffuse scattering close to the Bragg peak.

Laser fluence of 1.2 J m^{-2} was achieved by focusing both laser and X-rays down to a size of 35 μm full width at half maximum (fwhm). The X-ray focusing was used by a pair of Kirkpatrick–Baez silicon mirrors.

These measurements have been performed in the so-called low-alpha mode of the ANKA ring [31, 29], where the pulse length is reduced below 8 ps fwhm at an electron energy of 1.6 GeV. Therefore the X-ray energy of 5.5 keV was used inside an evacuated vessel.

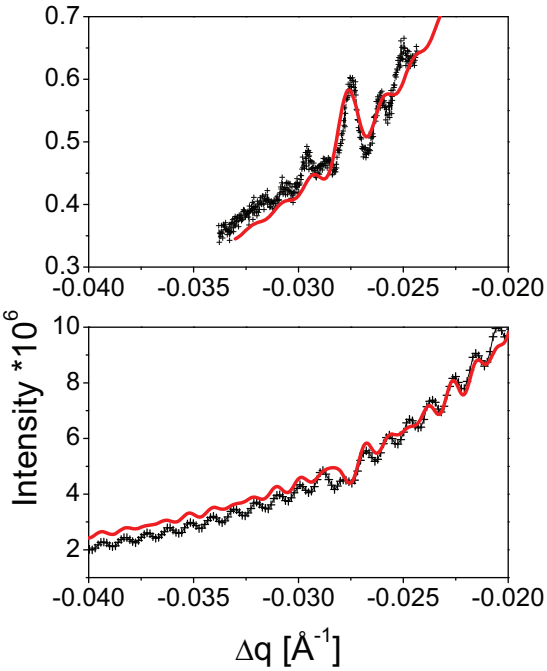

Figure 1 Static crystal truncation rod scattering of the symmetric (400) reflection of the silicon multilayer with alternating 28-Si and 29-Si (top) and the germanium multilayer with alternating 70-Ge and nat-Ge (bottom) as function of vertical momentum transfer Δq relative to the Bragg position close to the first-order superlattice reflection. The lines are simulations.

2.5 Static X-ray scattering Structure characterization was performed at the beamline SCD at ANKA with a monochromatic X-ray beam at 8.9 keV, a six-circle diffractometer and a linear directly-converting pixel detector (Mythen, Dectris). X-ray reflectivity allowed for a precise determination of gold layer quality and thickness [25], while the diffuse scattering close to the Bragg peaks of Si and Ge served to determine multilayer periods and quality.

Figure 1 shows a part of the symmetric crystal truncation rod of the silicon multilayer as well as the germanium layer structure. The curves show a faint oscillatory modulation. At around 0.027 Å^{-1} a stronger excursion from the otherwise slow decay with distance from the Bragg point is seen. Both features can be simulated quantitatively by dynamic X-ray diffraction theory [32, 33] by assuming (i) a perturbation of lattice spacing at the interface between the layer stack (multilayer or epilayer) and substrate; (ii) a periodic modulation of the strain within the multilayer stack of $\pm\ 1.9\times10^{-5}$ for silicon and $\pm\ 1.9\times10^{-5}$ for germanium with the period of (9.7 + 9.7) nm for silicon and (11.3 + 11.3) nm for germanium. Therefore, some defects may be present at the interface between the substrate and layer structures related to the growth initiation. These defects should act on the thermal properties of both multilayer sample and reference in the same way. Importantly the low amount of strain between the isotopic layers is in the range of the isotope lattice parameters changes and demonstrates the high epitaxial quality

of the stack [34]. Secondary ion mass spectroscopy [27, 7] shows well separated isotopic layers within the stacks.

2.6 Numerical procedures Phonon dispersion relations have been calculated according to the transfer matrix approach of a linear chain as described by Ezzahri et al. [8]. The key parameter is the longitudinal speed of sound, respectively, the impedance mismatch through different masses of the isotopes. This mismatch directly allows to estimate the gaps of the forbidden band of non-propagating phonons due to the zone folding. The gap scales with $(Z_A - Z_B)/\sqrt{(Z_A \cdot Z_B)}$ with Z_A and Z_B being the impedances of the sublayers [8]. With an assumption of 1.8% acoustic mismatch [9] the gaps for the present germanium isotope modulation are 1.4 GHz for the zone edge at $q = \pi/D$ and 42 MHz for the zone center at $q = 2\pi/D$. These values are extremely small in comparison to the phonon frequencies at these points (108 and 218 GHz).

Time-domain thermal conduction close to a heated surface in a layered system with transport only perpendicular to the surface is calculated by the so-called transmission-line approach [35, 36]. In essence, this is an analytical method for calculating the heat transfer by the diffusion equation by using the Laplace transform. Additionally the Stehfest numerical approximation for the transform is used. Individual layers are introduced via their thermal conductance and diffusivity as (2×2) matrix. Thermal interface conductance is introduced in a similar way. Finally the temperature in Laplace space is calculated by multiplying the matrices and backtransforming a function thereof to derive the temporal temperature decay of the top (heated layer). Three layers, gold top layer, multilayer stack, and substrate (semi-infinite) are used, but the approach can be generalized to an arbitrary number of layers.

Bulk conductivity and the thermal interface conduction between gold layer and semiconductor are determined, respectively checked for the epilayer sample and held fixed for the simulation of the multilayer sample, where only the conductivity of the multilayer stack is varied. The best fit value can be determined by a least squares determination and finding the minimum. This plot is shown as inset in Fig. 2. This returns an effective thermal conductivity of the complete stack, including any bulk or interface effects therein.

For an easy graphical estimation we derived the difference in transient heating between the multilayer sample and the reference epilayer sample, with the maximum expansion (maximum gold film temperature) fixed to 1. Thus, a reduced thermal conductivity of the multilayer would lead to a positive difference at time scales where the gradient in temperature is high in the multilayer stack. Figure 2 displays this difference together with a simulation of the change in effective thermal conductivity in the multilayer stack.

3 Results and discussion The aim of the isotopic modulation in our case is the modification of the thermal conductivity of the material by tailoring the phonon transport. In fact, our earlier studies have already shown that conductivity

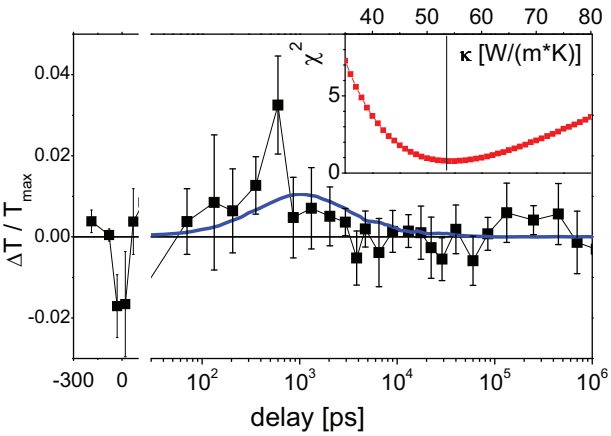

Figure 2 Relative change of transient thermal expansion of the heated gold layer on top of the germanium multilayer as compared to the reference epilayer in a synchronous pump–probe experiment. The line is a simulation according to the transfer-line model with an assumed change of effective thermal conductivity within the multilayer stack of 54 W/(m·K) as derived as minimal value of the least squares of the difference (χ^2) between experiment and simulation. The corresponding least squares curve is shown as inset.

can be reduced significantly in these multilayer structures. The amount of reduction still varies with samples, but some 60% of reduction has been found in silicon multilayers with isotopes 28/29 and 28/30 pairs [7, 37]. This number, while in absolute terms not a breakthrough, is nevertheless astonishing if one considers the minor mass contrast and thus minimal acoustic impedance of the stack. As pointed out in [8], a first estimate of this effect can be given by calculating phononic stop bands from the acoustic impedance (of the longitudinal phonons).

In a more rigorous way, the change of thermal conductivity is predicted by executing the integral over all phonon modes including their occupancy and velocity [11]. Reduction of transport is thus related to the modified band structure with both the appearance of stop bands and the reduction of group velocity close to them. On the basis of this formalism a reduction of the thermal conductivity by the multilayers can be predicted. If the phonon lifetime is not changed one derives a theoretical change in conductivity of, e.g., 1.5% for the germanium layers, which is way below the sensitivity of observation. In Fig. 2 the change of heat conduction of the Ge multilayer compared to the epilayer is displayed and simulated by a conductivity of (54 ± 4) W/(m·K), which represents reduction by 10%. This change is less than the earlier observations on silicon, however, the acoustic mismatch being lower and the lower bulk conductivity of germanium masking a subtle effect, this is still interesting. In fact, neglecting the influence of the layered structure on the phonon mean free path (or lifetime) is a too strong simplification. First of all, with less-than-perfect interfaces point scattering of phonons can occur, which reduces phonon lifetime and thus conductivity. It has been shown [38] that intermixed interfaces lead to a further depression of conductivity. For

stronger intermixing the limit can be the conductivity of a random alloy of isotopes.

On the other hand, the molecular dynamics studies also show a minimum in conductivity at a period length of 3 nm for silicon isotopes. This is a clear indication of the crossover between coherent and incoherent transport. Furthermore, it seems that aperiodic layering can further reduce thermal conductivity even below the alloy limit. Thus, not only incoherent (defect) scattering is responsible for the reduction in conductivity, but also multilayer-related scattering processes.

One of these processes is *Umklapp* scattering. Indeed at room temperature or above *Umklapp* scattering is the dominating contribution. Conventional *Umklapp* scattering occurs, when the phonon wave vector of an elastic scattering process exceeds the Brillouin zone and is therefore folded back with reversed direction.

In multilayers phonon band structure is characterized by a secondary Brillouin zone boundary introduced by the new artificial periodicity. This new mini zone should represent a similar obstacle to phonon propagation. Indeed the influence of mini-*Umklapp* processes has been discussed earlier [39–42].

To clarify the phonon dynamics ultrafast pump–probe measurements have been conducted. Laser spectroscopy allows for a very high time resolution and moderate technical complexity. On the other hand, the probing mechanism is often ambiguous, the momentum transfer not sufficient for mapping the band structure and the optical response unspecific.

We have employed ASOPS with high stability and low detection limit. Figure 3 displays the results on the 28/29 silicon multilayer structure. Transient modulations of the optical reflectivity are weak (in the range of 10^{-7} after removal of the prompt electronic contribution). Nevertheless, the Fourier transform of the temporal trace shows a peak distribution. When comparing this distribution to the mini-band structure as calculated for this structure, one can recognize matching features. The strongest peak at 209 GHz (4.78 ps period) coincides with the zone-edge, where the acoustic phonon branch is being folded back. A much lower peak appears at the zone-center phonon at 420 GHz. This zone-center phonon has been observed frequently in multilayer structures and is identified by a non-propagating phonon mode with multilayer periodicity [17]. High-order modes (such as 3rd order) of this mode can be identified as well at optimized background subtraction. The mode at 209 GHz is not expected to be observed in a Raman-type process, as the momentum transfer q of the probe light is here far below the zone-edge momentum transfer of π/D. Therefore ASOPS can not entirely clarify the assignment.

The germanium multilayer has been examined in an analogous fashion ((see Fig. 4). The transient reflectivity is dominated by one strong oscillation with amplitude of $>10^{-6}$. The stronger response is understandable by the considerably lower penetration depth of 800 nm light in germanium (600 nm versus 12 μm in silicon) and thus higher excitation density. The Fourier transform locates the oscillation mode

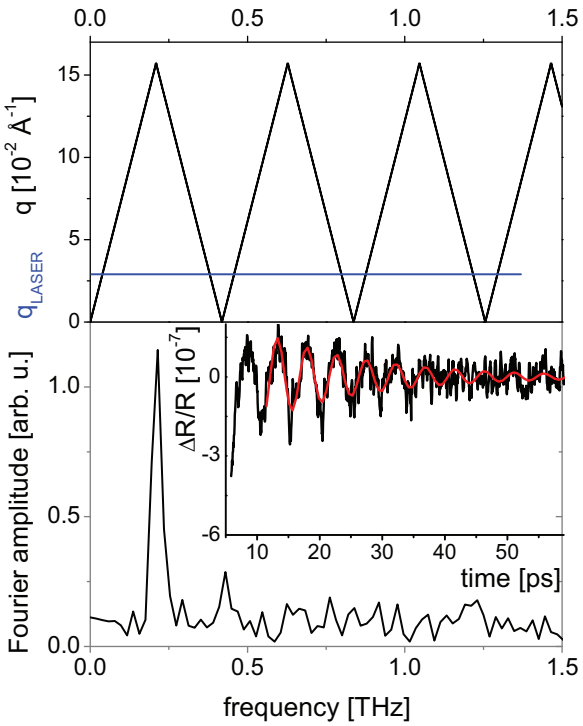

Figure 3 Top: Dispersion relation of a silicon crystal with superstructure of period $D = 19.4$ nm, with the momentum transfer of the longitudinal acoustic phonon along the ⟨100⟩ direction plotted as function of the frequency. The horizontal line in the top figure marks the momentum transfer of the probe light in the chosen reflection geometry. Bottom: Fourier transform of the transient light reflection from the surface (inset) from ASOPS. The inset shows the time-domain reflectivity together with a sinusoidal fit with 4.78 ps period.

at 55.5 GHz, which is close the predicted 55.2 GHz for a Raman-type excitation of an unfolded propagating acoustic mode. Strictly speaking this mode is not visible via a Raman process, but via the interference between the surface and the propagating sound wave in the bulk. This is also called Brillouin oscillation [8]. One can easily imagine that the lower excitation density in silicon is the reason for the absence there. As this mode is strong in germanium it is difficult to extract other modes. Nevertheless, one can find a weak peak at 108 GHz, again coinciding with the zone-edge modes of the folded band structure. It could be verified that this tiny mode disappears using the reference epilayer.

ASOPS consequently shows several modes, which correlate to folded and unfolded modes. The mechanism is an excitation of coherent phonons by a displacive excitation through ultrafast heating. The dominance of another mode is found, whose frequency coincides with the zone-edge. It is probably efficiently populated by phonon–phonon scattering (*Umklapp* processes). In order to verify the assignment in the dispersion relation we conducted time-resolved X-ray scattering in a similar fashion to ASOPS. Here, the momentum transfer is defined by the detuning of the scattering vector from the Bragg point, i.e., the (400) reflection in germanium.

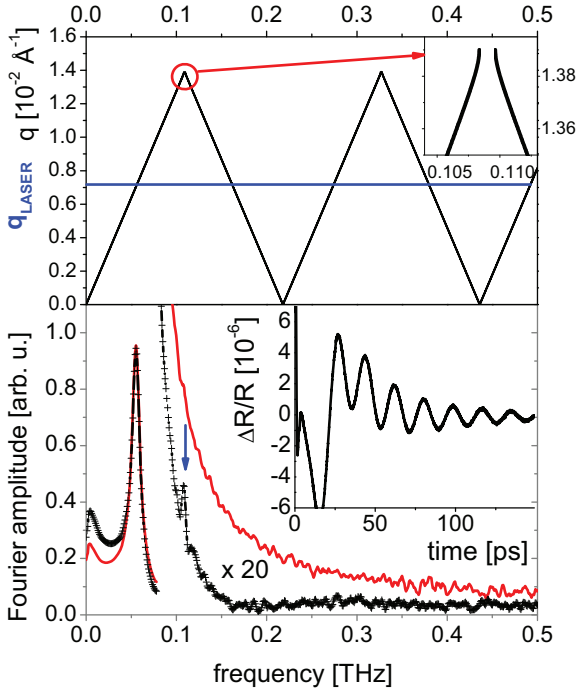

Figure 4 Top: Dispersion relation of a germanium crystal with superstructure of period $D = 22.6$ nm, with the momentum transfer of the longitudinal acoustic phonon along the ⟨100⟩ direction plotted as function of the frequency. The horizontal line marks the momentum transfer of the probe light in the chosen reflection geometry. A zoom of the zone-edge region at 110 GHz is shown as inset. Bottom: Fourier transform of the time-domain transient reflectivity in the ASOPS experiment of a Ge multilayer (black crosses) and the reference epilayer (red line). The arrow highlights the peaks due to zone-edge excitation. The inset shows part of the time-domain reflectivity.

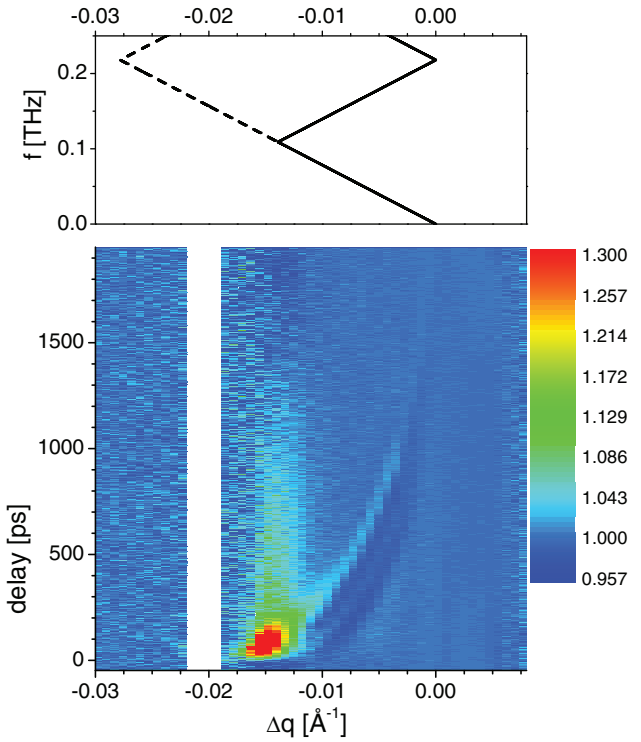

Figure 5 Dispersion relation (top) and false color representation (bottom) of the transient change in X-ray scattering close to the (400) reflection of the germanium multilayer as function of temporal delay between laser and X-ray pulse and the momentum transfer Δq relative to the Bragg position from the ASOXS experiment. The full line in the dispersion relation is the folded scheme, while the dashed line marks the extended dispersion.

With the short wavelength of the X-rays the necessary angular detuning is only a few tenths of a degree. The observed frequency of 108 GHz translates into a vibration period of 9.2 picoseconds and should just be resolved in the low-alpha mode at the synchrotron ANKA [29, 30]. It is known that phonon modes can directly be resolved in time domain and give rise to increased intensity at the corresponding angular deviation from the Bragg point [43].

The color-coded map of changes of X-ray intensity close to the Bragg point is depicted in Fig. 5 within the relevant momentum transfer and the temporal delay of 0–2000 ps. Two features dominate the change in scattering. First, there is a streak of additional intensity at 0.014 Å^{-1} , which starts shortly after excitation (delay = 0) and extends up to 1 ns, but with peaked intensity only in the range of 10–150 ps. The second feature is a stripe of increased (light blue) and decreased intensity that also starts at $q = 0.018$ Å^{-1}, but shifts gradually in momentum to end at the Bragg peak ($q = 0$) at some 1200 ps. The latter trace is an excitation of a propagation pulse of coherent phonons into the bulk of the material. In other words, the localized excitation in a shallow region of the germanium crystal causes an expansion of this layer, which propagates into the bulk with speed of sound [44, 45], followed by a rarefaction wave. This depends in position and strength on the excitation density.

The first feature, however, being stationary in momentum, represents a distinct phonon mode that is excited at earliest delays [24, 46]. The momentum transfer of q coincides with the zone edge position in the germanium multilayer. In contrast, we do not find any signature at the zone-center position at $q = 0.027$ Å^{-1}. Reason might be the lower signal-to-noise ratio at the lower intensity at higher momentum transfer or the less efficient excitation. Excitation of the zone-edge phonon seems to be enhanced through the coherent phonon wavepacket, as lowering the excitation density also reduces the stationary streak.

An oscillation could not be observed, although time resolution would just be at the limit to resolve the 9.2 ps period. A part of the limited resolution is due to the tight overlap of both laser and X-ray spots on the sample. They are both of the same size of 0.035 mm, so that the X-rays probe a gradient in excitation. The seemingly doubling of the phonon wavepacket streak (second feature below 500 ps) stems from this limitation. Also, if the interaction indeed involves an *Umklapp* process, this would be incoherent and thus not having a fixed phase relative to the excitation.

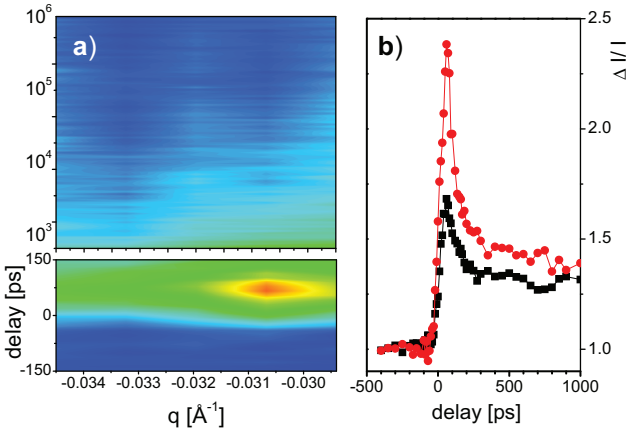

Figure 6 False color representation (a) and selected delay traces (b) of pump-laser induced intensity change at a shift angle $\Delta\theta$ relative to the Ge(400) Bragg reflection of a isotope-modulated Ge superlattice with high laser fluence and 100 ps time resolution (in synchronous mode). The delay traces are cut at 0.0306 Å^{-1} (dots) and 0.0331 Å^{-1} (squares).

A synchronous pump–probe scattering experiment has been conducted with kHz repetition rate and 100 ps X-ray pulses at a much higher excitation density (800 versus 1.2 J m^{-2}). The results are shown in Fig. 6. Here, indeed a transient scattering maximum at picosecond delay and $q = 0.0305$ Å^{-1} is observed, which again points toward a link between excitation density and excitation of finite momentum phonons. The time streak at the right side in Fig. 6 shows a time-resolution limited peak. This shape underlines the non-thermal nature of the excitation as a thermal heating excitation does only relax with the time scale of the heat transfer to bulk, which appears in the 2–5 nanosecond range.

Importantly, X-ray scattering corroborates the finding of defined phonons modes with laser excitation. The modes, which coincide in frequency with a zone-edge phonon are found in the X-ray dispersion map at the same q position. Therefore, it is concluded that zone-edge phonons can be excited strongly with laser excitation, while no particular mechanism other than an *Umklapp* process is known for this selective excitation. Therefore *Umklapp* processes should be considered as important aspect of energy flow in this system. The fact that zone-edge phonons have not frequently been observed earlier may be related to the low momentum transfer, favoring sensitivity to zone-center mode. We also believe that the isotope multilayers represent an extremely pure model system with the absence of spatially modulated absorption or strain or higher density of defects. In such a system, the subtle symmetry breaking due to the mass variation can unbury this effect from other influences.

4 Summary The ultrafast thermal and phononic response of isotopically modulated silicon and germanium multilayers has been investigated by means of femtosecond spectroscopy and ultrafast X-ray scattering. The multilayered structure can serve as degree of freedom of tuning thermal transport, in particular as it decouples thermal from electronic properties. The mechanisms behind this modification are subtly and counteracting. On the one hand, coherent transport in terms of Bloch waves favors ballistic phonon transport (in particular at lower temperatures), whereas at higher temperatures the reduction of conductivity may be due to phonon stop bands, which, however do not explain the magnitude of transport. We have shown that incoherent transport in terms of *Umklapp* processes at the mini-zone boundary are one mechanism that may contribute to lower conductivity. While taking advantage of the periodicity (coherence) of the multilayer structure it is still an incoherent effect, as propagating phonons scatter in individual multiphonon events under contribution of a wave vector $q = \pi/D$ of the artificial lattice. Looking ahead it will be important to disentangle the different effects of the layer structure, in seeing for instance the effect of periodic versus aperiodic arrangements or as function of temperature.

Acknowledgements This project is supported by German Science Foundation DFG under contract "Isotherm" within the priority program SPP 1386, within the Heisenberg fellowship of A. Plech and H. Bracht and within the Helmholtz-Association topic "Research with photons, ions and neutrons." We acknowledge beamtime and support by ESRF (beamline ID09b) and ANKA (beamlines SCD, SUL-X) and the Difflab at ANKA. Partial support by the SFB 767 is also acknowledged. We are grateful for profound help and support by N. Hiller, S. Ibrahimkutty, D. Khakhulin, N. Smale, S. Stankov, M. Wulff, and M. Zakharova. E. E. Haller and J. W. Ager were supported by the Director, Office of Science, Office of Basic Energy Sciences, Materials Sciences and Engineering Division, of the U.S. Department of Energy under Contract No. DE-AC02-05CH11231.

References

[1] G. J. Snyder and E. S. Toberer, Nature Mater. **7**, 105 (2008).
[2] S. Chakraborty, C. A. Kleint, A. Heinrich, C. M. Schneider, J. Schumann, M. Falke, and S. Teichert, Appl. Phys. Lett. **83**, 4184 (2003).
[3] M. N. Luckyanova, J. Garg, K. Esfarjani, A. Jandl, M. T. Bulsara, A. J. M. Aaron J. Schmidt, S. Chen, M. S. Dresselhaus, Z. Ren, E. A. Fitzgerald, and G. Chen, Science **338**, 936 (2012).
[4] J. Ravichandran, A. K. Yadav, R. Cheaito, P. B. Rossen, A. Soukiassian, S. J. Suresha, J. C. Duda, B. M. Foley, C. H. Lee, Y. Zhu, A. W. Lichtenberger, J. E. Moore, D. A. Muller, D. G. Schlom, P. E. Hopkins, A. Majumdar, R. Ramesh, and M. A. Zurbuchen, Nature Mater. **13**, 168 (2014).
[5] M. V. Simkin and G. D. Mahan, Phys. Rev. Lett. **84**, 927 (2000).
[6] R. Venkatasubramanian, Phys. Rev B **61**, 3091 (2000).
[7] H. Bracht, S. Eon, R. Frieling, A. Plech, D. Issenmann, D. Wolf, J. Lundsgaard Hansen, A. Nylandsted Larsen, J. Ager III, and E. E. Haller, New J. Phys. **16**, 015021 (2014).
[8] Y. Ezzahri, S. Grauby, J. M. Rampnoux, H. Michel, G. Pernot, W. Claeys, S. Dilhaire, C. Rossignol, G. Zeng, and A. Shakouri, Phys. Rev. B **75**, 195309 (2007).
[9] G. Bastian, A. Vogelsang, and C. Schiffmann, J. Electron. Mater. **39**, 9 (2010).

[10] Y. Chen, D. Li, J. R. Lukes, Z. Ni, and M. Chen, Phys. Rev. B **72**, 174302 (2005).
[11] S. Tamura, Y. Tanaka, and H. J. Maris, Phys. Rev. B **60**, 2627 (1999).
[12] G. Chen, Phys. Rev. B **57**, 14958 (1998).
[13] J. Garg, N. Bonini, and N. Marzari, Nano Lett. **11**, 5135–5141 (2011).
[14] Y. Wang, C. Gu, and X. Ruan, Appl. Phys. Lett. **106**, 073104.
[15] T. Mishina, Y. Iwazaki, Y. Masumoto, and M. Nakayama, Solid State Commun. **107**, 281 (1998).
[16] A. Bartels, T. Dekorsy, H. Kurz, and K. Köhler, Phys. Rev. Lett. **82**, 1044 (1999).
[17] M. Bargheer, N. Zhavoronkov, Y. Gritsai, J. C. Woo, D. S. Kim, M. Woerner, and T. Elsaesser, Science **306**, 1771 (2004).
[18] A. Bartels, F. Hudert, C. Janke, T. Dekorsy, and K. Köhler, Appl. Phys. Lett. **88**, 041117 (2006).
[19] S. M. Lee, D. G. Cahill, and R. Venkatasubramanian, Appl. Phys. Lett. **70**, 2957 (1997).
[20] M. Herzog, D. Schick, P. Gaal, R. Shayduk, C. V. Korff Schmising, and M. Bargheer, Appl. Phys. A **106**, 489 (2012).
[21] C. Colvard, T. A. Gant, M. V. Klein, R. Merlin, R. Fischer, H. Morkoc, and A. C. Gossard, Phys. Rev. B **31**, 2080 (1984).
[22] J. Spitzer, T. Ruf, M. Cardona, W. Dondl, R. Schorer, G. Abstreiter, and E. E. Haller, Phys. Rev. Lett. **72**, 1565 (1994).
[23] T. Kojima, R. Nebashi, K. M. Itoh, and Y. Shiraki, Appl. Phys. Lett. **83**, 2318 (2003).
[24] M. Trigo, Y. M. Sheu, D. A. Arms, J. Chen, S. Ghimire, R. S. Goldman, E. Landahl, R. Merlin, E. Peterson, M. Reason, and D. A. Reis, Phys. Rev. Lett. **101**, 025505 (2008).
[25] D. Issenmann, S. Eon, N. Wehmeier, H. Bracht, G. Buth, S. Ibrahimkutty, and A. Plech, Thin Solid Films **541**, 28 (2013).
[26] F. Schotte, S. Techert, P. A. Anfinrud, V. Srajer, K. Moffat, and M. Wulff, Third-Generation Hard X-ray Synchrotron Radiation Sources (John Wiley and Sons, Inc., Berlin, 2002).
[27] H. Bracht, N. Wehmeier, S. Eon, A. Plech, D. Issenmann, J. Lundsgaard Hansen, A. Nylandsted Larsen, J. Ager III, and E. Haller, Appl. Phys. Lett. **101**, 064103 (2012).
[28] V. Kotaidis, T. Dekorsy, S. Ibrahimkutty, D. Issenmann, D. Khakhulin, and A. Plech, Phys. Rev. B **86**, 100101 (2012).
[29] S. Ibrahimkutty, D. Issenmann, S. Schleef, A. S. Müller, Y. L. Mathis, B. Gasharova, E. Huttel, R. Steininger, J. Göttlicher, T. Baumbach, A. Bartels, C. Janke, and A. Plech, J. Synchrotron Radiat. **18**, 539 (2011).
[30] D. Issenmann, S. Ibrahimkutty, R. Steininger, J. Göttlicher, T. Baumbach, N. Hiller, A. S. Müller, and A. Plech, J. Phys.: Conf. Ser. **425**, 092007 (2013).
[31] M. Abo-Bakr, J. Feikes, K. Holldack , G. Wüstefeld, and H. W. Hübers, Phys. Rev. Lett. **88**, 254801 (2002).
[32] O. M. Lugovskaya and S. A. Stepanov, Sov. Phys. – Crystallogr. **36**, 478 (1991).
[33] S. Stepanov, X-ray server: An online resource for simulations of X-ray diffraction and scattering, http://sergey.gmca.aps.anl.gov/x0h.html.
[34] C. Herrero, Solid State Commun. **110**, 243 (1999).
[35] G. Chen and P. Hui, Thin Solid Films **339**, 58 (1999).
[36] Z. X. Huang, Z. A. Tang, J. Yu, and S. Bai, Physica B **406**, 818 (2011).
[37] S. Eon, H. Bracht, A. Plech, J. Lundsgaard Hansen, A. Nylandsted Larsen, J. W. Ager III, and E. E. Haller, Phys. Status Solidi A, submitted (2015).
[38] R. Frieling, M. Radek, S. Eon, H. Bracht, and D. E. Wolf, Appl. Phys. Lett. **105**, 132104 (2014).
[39] S. Y. Ren and J. D. Dow, Phys. Rev. B **25**, 3750 (1982).
[40] D. J. Lockwood, M. W. C. Dharma-wardana, J. M. Baribeau, and D. C. Houghton, Phys. Rev. B **35**, 2243 (1987).
[41] A. Ward and D. A. Broido, Phys. Rev. B **77**, 245328 (2008).
[42] Y. R. Yang, X.-H. Yan, J.-X. Cao, Y. Xiao, Y.-L. Mao, J. Xiang, and H.-L. Yu, Chinese Phys. **13**, 2109 (2004).
[43] A. Bojahr, M. Herzog, S. Mitzscherling, L. Maerten, D. Schick, J. Goldshteyn, W. Leitenberger, R. Shayduk, P. Gaal, and M. Bargheer, Opt. Express **21**, 21188 (2013).
[44] D. A. Reis, M. F. DeCamp, P. H. Bucksbaum, R. Clarke, E. Dufresne, M. Hertlein, R. Merlin, R. Falcone, H. Kapteyn, M. M. Murnane, J. Larsson, T. Missalla, and J. S. Wark, Phys. Rev. Lett. **86**, 3072 (2001).
[45] K. Sokolowski-Tinten, C. Blome, C. Dietrich, A. Tarasevitch, M. Horn von Hoegen, D. von der Linde, A. Cavalleri, J. Squier, and M. Kammler, Phys. Rev. Lett. **87**, 225701 (2001).
[46] M. Herzog, A. Bojahr, J. Goldshteyn, W. Leitenberger, I. Vrejoiu, D. Khakhulin, M. Wulff, R. Shayduk, P. Gaal, and M. Bargheer, Appl. Phys. Lett. **100**, 094101 (2012).

